

Received January 22, 2020, accepted February 7, 2020, date of publication February 20, 2020, date of current version February 28, 2020.

Digital Object Identifier 10.1109/ACCESS.2020.2975125

Maxwell Model-Based Null Space Compliance Control in the Task-Priority Framework for Redundant Manipulators

LE FU¹ AND JIE ZHAO¹

State Key Laboratory of Robotics and System, Harbin Institute of Technology, Harbin 150001, China

Corresponding author: Jie Zhao (jzhao@hit.edu.cn)

This work was supported in part by the Major Research Plan under Grant 91648201, and in part by the Foundation for Innovative Research Groups of the National Natural Science Foundation of China under Grant 51521003.

ABSTRACT Improving robot performance while simultaneously ensuring compliance and human safety has been appealing for a long time and remains a challenge. To this end, we propose a new approach for kinematic control of redundant manipulators to deal with multiple prioritized tasks and at the same time produce a novel compliance behavior in the null space of main task. Different from typical Voigt model based compliance control methods, the compliance control approach proposed in this paper is based on Maxwell model, which shows superior performance on impact absorption and contact reducing than its counterparts. In comparison with typical compliance control, the annoying and even harmful return force is removed and human comfortableness can be improved consequently. Besides, this novel compliance control method is implemented in the null space of higher priority task without disturbing the main end-effector task. The effectiveness of our approach has been practically evaluated and verified in experiments on a 7 DOF redundant collaborative robot manipulator. A novel cushion-like and plastic deformed whole body compliance has been realized while the continuity and quality of robot main task have been maintained. Promisingly, the approaches proposed in this paper are general and manipulator independent, which can also be applied to other emerging collaborative and even hyper redundant manipulators. Besides, research results of this work can also potentially inspire other robotic research related with human robot friendly interaction and collaboration.

INDEX TERMS Multi-prioritized framework, null space compliance control, Maxwell model, plastic deformation.

I. INTRODUCTION

The past several decades have witnessed the trend that robots work alongside human, share a common workspace without separated and safeguarded fences or barriers. The appealing combination of human strength on intelligence and adaptivity with advantages of robots on accuracy and repeatability have been desired for quite a long time. As illustrated in Fig. 1, a robot manipulator works on an assembling task with human coexistence and physical interaction on its body. Due to human presence, the working environment of robots have changed from structured and known in advance to unstructured and even totally unpredictable. Considering the intentional and accidental physical contacts or impacts may

happen in scenarios like Fig. 1, hazard and injury to human may occur consequently. Therefore, ensuring human safety and simultaneously keeping robot main task performance undisturbed and efficient are highly demanded and remain a challenge.

Nowadays, collaborative robots(also known as Cobot [1]), which are designed to intentionally interact with humans in shared work space, have become a new trend in global robot market and applications. Besides, human-like and hyper-redundant robots are emerging and attracting more and more attention of robotic community. Theoretically, every robot manipulator may become redundant depending on desired tasks. In general spatial task with six degree of freedom, a seven or more joints robot manipulator is often considered as inherent redundant [2]. In other cases, a six or less joints manipulator may become functional redundancy when the

The associate editor coordinating the review of this manuscript and approving it for publication was Hui Xie¹.

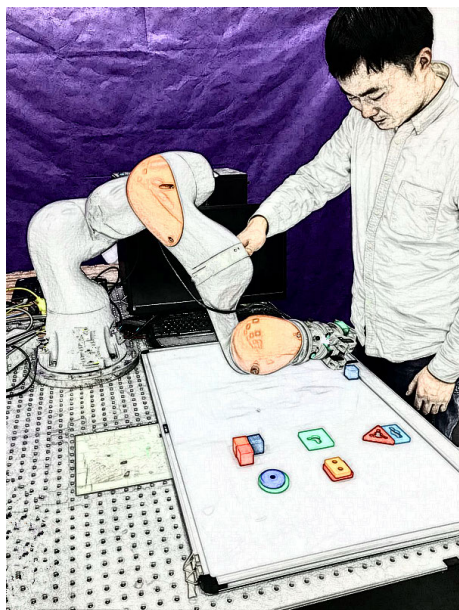


FIGURE 1. Scenario of human robot collaboration with physical interaction.

dimension of operational space is greater than the dimension of specific task space, such as end-effector position regulation with no constraints on orientation. Although redundancy may bring difficulties on a number of issues including mechanical design and inverse kinematic problems, redundant robots still have significant advantages on singularity avoidance, performance optimization, etc. Exploiting the remaining degrees of freedom apart from those required in main task, complex and dexterous functions and movements can be achieved by proper redundancy resolutions. For example, an improved human-robot collaborative control scheme, exploiting the redundancy to guarantee a remote center of motion (RCM) constraint and to provide a compliant behavior for the medical staff, has been proposed in [3]. Considering the issue with safety and accurate surgical task execution, the redundancy of the manipulator is also exploited to provide a flexible workspace for nurses or other staff (assisting physicians, patient support) [4]. In order to achieve a human-like behavior, a novel deep convolutional neural network (DCNN) structure for reconstruction enhancement and reducing on-line prediction time to manage redundancy control of a 7 DoFs anthropomorphic robot arm has been reported in [5].

Generally, different first-order redundancy resolutions can be divided into two main categories, namely optimization based methods [6], [7] and task argumentation approaches [8], [9]. Besides, redundancy can be solved in second-order or acceleration level, taking the dynamic issues into consideration [10]. Among those redundancy resolutions, multi priority is a framework to solve the conflict between robot end-effector task and the constrained tasks, by suitably assigning the given tasks into an order of priority and then satisfying the lower-priority task in the null space of

higher-priority task [11]. The basic idea is that the execution error of lower-priority task do not affect the higher-priority tasks. This framework is rather suitable for robots working with human in unstructured environment, since both the main end-effector task and other desired or unexpected tasks needed to tackle simultaneously. This paper is motivated to realize versatile robot movements based on the framework of multi-priority for redundant manipulators, with a special care of human safety. It is well known that compliance in robot systems plays an importance role in contact force reduction and limitation, making robot soft and improving human safety [12]. In this paper, we focus on the problem of ensuring the main execution of robot end-effector task and simultaneously realizing a null space compliance control to deal with those physical contracts in unstructured environments.

In practical implementations, compliance can be intrinsically realized in mechanical way [13], [14] [15]. The other way is referred as compliance control, including impedance control [16], admittance control [17] and their variants such as variable impedance learning in robot force based manipulation [18], adaptive impedance control by reinforcement learning in human robot cooperation [19]. Moreover, a force sensorless admittance control scheme using radial basis neural networks (NNs) for robotic manipulators to interact with unknown environments in the presence of actuator saturation has been proposed in [20]. For physical interaction and collision between robot manipulators and human arms, a force sensorless control scheme based on neural networks (NNs) has been developed in [21]. The majority of compliance methods mentioned above are based on a viscoelastic model, which termed Kelvin-Voigt (Voigt for short) model [22]. The characteristics of Voigt model is an elastic deformation behavior and a return force always generated, when external contact happens. This elastic deformation behaviors can cause several drawbacks: 1) unsafe and harmful in some situations: the main control goal of typical compliance control is exerting a desired relationship (termed as impedance and admittance) between external force and resultant displacements. Due to the elasticity of Voigt model, the elastic return force approximates a proportional relationship (Hooke's law) as $F_{return} \approx K_{stiffness} \cdot \Delta x$ in typical compliance control. If the stiffness $K_{stiffness}$ or the displacement Δx are large enough, the resultant elastic return force F_{return} may exceed the pain thresholds of human body to quasi static and transient contact, which have been studied by researchers from multi-disciplines [23], [24] and published as mandatory thresholds in the newest ISO safety standard for collaborative robots [25]. Therefore, human safety may not be guaranteed. 2) human comfortableness is limited during human robot physical interaction: also due to the annoying elastic return forces, human always feel be pushed backwards. These forces are in the opposite direction of intentional contact forces during human robot physical interaction. As a result, human robot interaction may not in a friendly way. 3) The safety and comfortableness of human may get worse when impact or accidental physical contacts happens. This is

determined by the inherent interconnections between spring and damper in the Voigt model.

Maxwell model is another linear viscoelastic model, which describes the plastic deformation behavior of material and substance [26]. According to the theory of Elastoplastic Mechanics, a plastic deformation can be acquired when external forces are applied, due to the particular constitutive relations of Maxwell model [27]. Other research works have verified that Maxwell model has a superior performance on contact reducing and impact absorption, compared with typical Voigt model [28]. In robotic related research, a Maxwell model based two-dimensional visual shock absorber with a spring based passive body and a damping controlled damper has been reported in [29]. The authors construct this shock absorber by imitating the series inter connection of Maxwell model. In their work, experiment results show that effectiveness of impact absorption of a fast rolling object without repelling it back. A Maxwell model based Cartesian space admittance control approach has been proposed and reported in our former work [30]. The experiment results show that a novel plastic deformation behavior of robot end-effector can be realized in Cartesian space and human comfortableness is improved during human robot interaction, due to the drawbacks of annoying even unsafe elastic return forces are overcome by the employment of Maxwell model.

Actually, one of our recent works has been presented and published in the proceedings of *2019 IEEE 4th International Conference on Advanced Robotics and Mechatronics (ICARM, Osaka, Japan)* [30]. Motivated by the discussions with many interested robotic specialists from different countries, the authors are encouraged to conduct further and deeper research. The main differences are that the former work realize a Cartesian space compliance control, whereas we propose a Maxwell model based null space compliance control approach to achieve a novel whole-body compliance while simultaneously ensuring robot main task undisturbed. The novelty of this null space compliance is that the advantages of Maxwell model on contact reducing and impact absorbing are fully exploited. The annoying and harmful return forces are also removed on a scale as large as whole body of robot manipulators. A novel cushion-like whole body compliance is realized without disturbing the robot main task. Therefore, human safety and comfortableness can be improved consequently.

The main contributions of this paper are given as follows:

- We derive a recursive form of kinematic multi-prioritized redundancy resolution. This scheme can decouple the desired complex tasks into multiple prioritized in pre-defined hierarchical architecture.
- In order to exploit the advantages of Maxwell model on contact reducing and impact absorption, based on this formulation, a Maxwell model based compliance control approach is designed in the null space of higher priority tasks. Besides, this method is general and manipulator independent.

- The methods proposed in this paper have been practically implemented and verified on a 7 DOF collaborative manipulator. Compared with typical Voigt model based compliance control, the annoying and even harmful elastic return forces are removed and human comfortableness get improved. The appealing combination of human safety demanded whole-body compliance and robot main task performance can be realized to a certain extent by our methods. To the best of the author's knowledge, this paper is the first one reported on this topic at present.

This paper is organized as follows: Some related preliminaries including the derivation of recursive form of velocity-based redundancy solution are recalled and given in Section 2, followed by typical Voigt model based compliance control method in Section 3. The Maxwell model based compliance control method we proposed is present in Section 4. Section 5 addresses the singularity and joint limits avoidance problems. Experiments verification, comparisons and discussions are given in Section 6. And section 7 concludes this paper.

II. PRELIMINARIES

A. COMPARISON OF TWO VISCOELASTIC MODELS

Viscoelasticity is a fundamental property of materials that exhibit viscous and elastic characteristics when forces applied. Voigt model and Maxwell model are two constitutive models of linear viscoelasticity [26]. As shown in Fig. 2, the main differences of these two models are the internal combination of spring and damper and also the explicit deformation behaviors. In the former one, Voigt model, the connection of spring and damper is parallel. According to the Hooke's law, the spring always generates return force when displacement observed, which resulting in an elastic deformation. On the contrary, the connection of spring and damper is changed into series, which leads to a plastic deformation after applied force removed.

The comparison of one-dimensional motion equations of two viscoelastic models when external contact force F applied are given as (1) and (2), respectively. M , C and K represent mass, damping and stiffness coefficients. As shown in Fig. 2, an equivalent expression exists on the condition that these coefficients of both two viscoelastic models are the same. The detailed mathematical formulations and dynamics property comparisons are presented in our former work [30].

$$M\ddot{x}_e + C\dot{x}_e + Kx_e = F \quad (1)$$

$$M\ddot{x}_e + KC^{-1}M\dot{x}_e + Kx_e = F + KC^{-1}\int Fdt \quad (2)$$

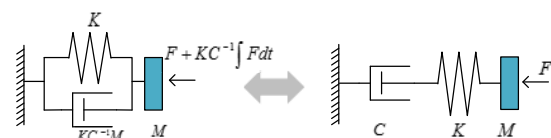


FIGURE 2. Two viscoelastic models and the equivalent transformation between them. left: Voigt model expression. right: Maxwell model expression.

B. GENERALIZED INVERSE AND ITS PROPERTIES

Recall that the task and joint space variables $x \in R^{m \times 1}$ and $q \in R^{n \times 1}$ in differential kinematics are related by $m \times n$ Jacobian matrix J and formulated as follows,

$$\dot{x} = J\dot{q} \quad (3)$$

If the inverse of J^{-1} exists and non-singularity is assumed, there is one solution to (3). But in general cases, there may result in no solution or an infinity of solutions. Under the assumption of kinematic redundant, more general solution of (3) can be expressed by the pseudo-inverse J^\dagger of the task Jacobian matrix J . In the sense of minimizing the residual norm $\|J\dot{q} - \dot{x}\|$, a least-squares general inverse is obtained, which leads to a general solution (4) for redundant case.

$$\dot{q} = J^\dagger \dot{x} + (I - J^\dagger J)\eta \quad (4)$$

If J is low-rectangular and full-rank, the pseudo-inverse J^\dagger can be formulated as $J^\dagger = J^T(JJ^T)^{-1}$; η represents for null-space joint velocity, which can be exploited to versatile joint velocities that produce the same end-effector task velocity \dot{x} .

The properties of the pseudo-inverse J^\dagger defined above are listed as follows.

$$\begin{aligned} JJ^\dagger J &= J, J^\dagger JJ^\dagger = J^\dagger, \\ (JJ^\dagger)^T &= JJ^\dagger, (J^\dagger J)^T = J^\dagger J \end{aligned} \quad (5)$$

C. VELOCITY BASED REDUNDANCY RESOLUTION IN RECURSIVE FORMULATION

As mentioned above, the general solution of redundancy (4) can be exploited for different purposes, such as singularity or obstacle avoidance, optimization of other performances and etc. By suitably designing the null-space joint velocity η , multiple tasks with predefined priorities can be achieved. Here, we start from two subtasks and formulate into more general and recursive form. Suppose the first and second priority tasks are denoted as $x_1 \in R^{m_1}$ and $x_2 \in R^{m_2}$ respectively. The consequent differential relationships are expressed as follows:

$$\dot{x}_i = J_i(q)\dot{q}, \quad i = 1, 2 \quad (6)$$

where $J_i(q) \triangleq \partial x_i / \partial q \in R^{m_i \times n}$ are the Jacobian matrices for the i_{th} task variables. Similar as (4), the general redundancy solution of the 1_{th} task is as follows.

$$\dot{q} = J_1^\dagger \dot{x}_1 + (I - J_1^\dagger J_1)\eta \quad (7)$$

Now, substitute (7) to (6) for the second task, we have

$$J_2(I - J_1^\dagger J_1)\eta = \dot{x}_2 - J_2 J_1^\dagger \dot{x}_1 \quad (8)$$

In the same way as (7), which minimizes the norm $\|\dot{x}_2 - J_2 \dot{q}\|$, the null-space velocity η can be expressed as

$$\eta = \bar{J}_2^\dagger (\dot{x}_2 - J_2 J_1^\dagger \dot{x}_1) + (I - \bar{J}_2^\dagger \bar{J}_2)\zeta \quad (9)$$

where $\bar{J}_2 = J_2(I - J_1^\dagger J_1)$, and $\zeta \in R^n$ is also an arbitrary null space velocity vector. Substitute (9) into (7), the redundancy solution of two prioritized tasks is as follows,

$$\dot{q} = J_1^\dagger \dot{x}_1 + \bar{J}_2^\dagger (\dot{x}_2 - J_2 J_1^\dagger \dot{x}_1) + (I - J_1^\dagger J_1)(I - \bar{J}_2^\dagger \bar{J}_2)\zeta \quad (10)$$

Repeat this procedure and generalize in a recursive form, we obtain

$$\dot{q}_i = \dot{q}_{i-1} + \bar{J}_i^\dagger (\dot{x}_i - J_i \dot{q}_{i-1}), \quad \dot{q}_1 = J_1^\dagger \dot{x}_1 \quad (11)$$

with $\bar{J}_i = J_i P_{i-1}^A$, where $P_i^A = I - J_i^A \bar{J}_i^A$ is the projector onto the null space of the following Jacobian $J_i^A = [J_1^T J_2^T \dots J_i^T]^T$.

It is noteworthy that this projection term $\bar{J}_i = J_i P_{i-1}^A$ allows task x_i to perform within the null space or higher priority tasks and ensure no affecting those higher priority tasks [31].

D. EXTERNAL FORCE ESTIMATION FOR NULL SPACE COMPLIANCE CONTROL

Generally, wrist force/torque sensors are becoming more and more popular and easy to be installed on robot flange. However, external contact forces acting in the null space of robot main task are more problematic and require observers or additional measurement. It is well known that impedance control is resolvable in torque-controlled robots without force measurement, on the condition of only stiffness and damping regulation without inertia shaping. However, joint external torques information is needed in our velocity-based compliance control case, which often referred to as admittance control [17].

A lot of torque estimation methods have been reported in literatures works. A Kalman filter based approach for external forces and torques estimation is presented in [32]. In there work, only motor current, joint angles and velocities signals are needed. Observer-based approaches have been proposed in [33], [34]. In this paper, we use a well-established external torques estimation method called *generalized momentum*, which is introduced for actuator fault detection [35]. This method has been exploited to human robot interaction control in [36]. Here, we brief the mathematical formulation as follows.

The dynamics model of a n joints robot manipulator with physical contact force is formulated as,

$$M(q)\ddot{q} + C(q, \dot{q}) + g(q) = \tau - \tau_{ext} \quad (12)$$

where, $q \in R^{n \times 1}$ represents the joint configuration, $M(q) \in R^{n \times n}$ is the inertia matrix, $C(q, \dot{q}) \in R^{n \times 1}$ is denoted for Coriolis and centrifugal forces, and $g(q) \in R^{n \times 1}$ is gravity term. Besides, $\tau \in R^{n \times 1}$ is the robot control torque and $\tau_{ext} \in R^{n \times 1}$ is the external torques resulting by physical contacts. According to the definitions in (12), the n dimensional residual vector r is defined as follows.

$$r(t) = K_{obs}(p(t) - \int_0^t (\tau + C^T \dot{q} - g + r(\sigma)) d\sigma) \quad (13)$$

where $p(t) = M\dot{q}$ is defined as the generalized momentum with $p(0) = 0$ and $r(0) = 0$. $K_{obs} \in R^{m \times n}$ is a positive definite matrix, which determines the dynamics of residual vector,

$$\dot{r} = -K_{obs}r - K_{obs}\tau_{ext} \quad (14)$$

From (14), we can see that the residual vector $r \approx \tau_{ext}$, by choosing proper gain K_{obs} . So this residual vector r can be treated as an estimation of the joint torques caused by external contact forces. Moreover, this approach is manipulator independent and can be used as redundant and non-redundant cases.

III. TYPICAL VOIGT MODEL BASED NULL SPACE COMPLIANCE CONTROL IN MULTI-PRIORITY FRAMEWORK

As emphasized above, our main purpose in this work is to achieve a Maxwell model based null space compliance for the sake of human safety while not disturb the main task. To this end, the desired compliance is designed in the null space of higher priority tasks. Therefore, we firstly formulate the null space compliance law in the joint space, and then project it into the multi-priority formulations in above subsection. It is noteworthy that the main concerns of this paper are based on kinematic control (i.e. position and velocity) of robot manipulators. The main reason is that plenty of existing literature works are formulated in torque level. Unfortunately, torque control interface is appealing but not so common as kinematic control interfaces, especially those commercial robot manipulators. Therefore, the following methods are general and manipulator independent, which means almost all robot manipulators including fixed and mobile ones are applicable.

For typical Voigt model based joint space compliance control, the desired compliance law in joint space is formulated as,

$$M_d(\ddot{q}_d - \ddot{q}) + C_d(\dot{q}_d - \dot{q}) + K_d(q_d - q) = \tau_{ext} \quad (15)$$

where $\dot{q}_d = \dot{q}_d(t) \in R^{n \times 1}$ is the desired joint velocity, and $M_d, C_d, K_d \in R^{n \times n}$ are all positive definite matrices, denoting the desired inertia, damping and stiffness, respectively. Transform (15) into Laplace form, we obtain

$$(M_d s + C_d + K_d/s)(\dot{q}_d - \dot{q}) = \tau_{ext} \quad (16)$$

Define the admittance filter as $A = M_d s + C_d + K_d/s$, then

$$\dot{q} = \dot{q}_d - A^{-1}\tau_{ext} \quad (17)$$

where $\dot{q} \in R^{n \times 1}$ is the joint velocities related to the external forces. Put (17) into the multi-prioritized framework recursive formulations (11) discussed in above section. The overall joint velocity control commands to robot velocity controllers can be derived accordingly.

For instance, in two-levels prioritized tasks, we have

$$\dot{q}_c = J_1^\dagger \dot{x}_1 + (I - J_1^\dagger J_1)(\dot{q}_d - A^{-1}\tau_{ext}) \quad (18)$$

It is mention-worthy that the desired null space velocity do not have so much practical usage and is non-integrable [37].

Normally, we let $\dot{q}_d = 0$, and then (18) can be simplified as follows:

$$\dot{q}_c = J_1^\dagger \dot{x}_1 - (I - J_1^\dagger J_1)A^{-1}\tau_{ext} \quad (19)$$

The overall joint velocities control commands for three-levels prioritized tasks are expressed as (20), in which the desired compliance (15) is designed as the third task level. That means the joint velocities caused by external contact torques are constrained in the null space of the other two task x_1 and x_2 with higher priorities. Theoretically, tasks with higher priorities are not disturbed by the desired compliance control scheme. More prioritized task levels can be solved with the help of the recursive form (11).

$$\begin{aligned} \dot{q} = & J_1^\dagger \dot{x}_1 + \bar{J}_2^\dagger (\dot{x}_2 - J_2 J_1^\dagger \dot{x}_1) \\ & + (I - J_1^\dagger J_1)(I - \bar{J}_2^\dagger \bar{J}_2)(A^{-1}\tau_{ext}) \end{aligned} \quad (20)$$

IV. MAXWELL MODEL BASED NULL SPACE COMPLIANCE CONTROL IN MULTI-PRIORITY FRAMEWORK

As investigated in section 2.1, the desired relationships between external force and displacement of both viscoelastic models are totally different. In this section, we propose a Maxwell model based null space compliance control approach in multi prioritized framework. Firstly, the desired joint space compliance is designed as follows,

$$\begin{aligned} M_d(\ddot{q}_d - \ddot{q}) + K_d C_d^{-1} M_d(\dot{q}_d - \dot{q}) + K_d(q_d - q) \\ = \tau_{ext} + K_d C_d^{-1} \int \tau_{ext} dt \end{aligned} \quad (21)$$

where $\ddot{q}_d, \dot{q}_d, q_d \in R^{n \times 1}$ is the desired joint acceleration, velocity, and position, respectively. $M_d, C_d, K_d \in R^{n \times n}$ are all positive definite matrices, representing the desired inertia, damping and stiffness. Similarly, transform (21) into Laplace expression and we obtain,

$$\begin{aligned} (M_d s + K_d C_d^{-1} M_d + K_d/s)(\dot{q}_d - \dot{q}) \\ = \tau_{ext} + K_d C_d^{-1} \int \tau_{ext} dt \end{aligned} \quad (22)$$

Denote the Maxwell model based admittance filter as $A' = M_d s + K_d C_d^{-1} M_d + K_d/s$, then

$$\dot{q} = \dot{q}_d - A'^{-1}(\tau_{ext} + K_d C_d^{-1} \int \tau_{ext} dt) \quad (23)$$

where $\dot{q} \in R^{n \times 1}$ is the resultant joint velocities caused to the external forces. Substitute (23) into the multi-prioritized framework recursive formulations (11) discussed above. The overall joint velocity control commands sent to robot velocity controllers can be derived accordingly. For two-levels prioritized tasks, we have

$$\begin{aligned} \dot{q}_c = & J_1^\dagger \dot{x}_1 + (I - J_1^\dagger J_1)(\dot{q}_d - A'^{-1}\tau_{ext} \\ & + K_d C_d^{-1} \int \tau_{ext} dt) \end{aligned} \quad (24)$$

Generally, let the desired null space velocity $\dot{q}_d = 0$, and then (24) can be expressed as following.

$$\dot{q}_c = J_1^\dagger \dot{x}_1 - (I - J_1^\dagger J_1)A'^{-1}(\tau_{ext} + K_d C_d^{-1} \int \tau_{ext} dt) \quad (25)$$

The overall joint velocities control commands for three-levels prioritized tasks are expressed as (26), in which the desired compliance (21) is designed as the third task level. That means the joint velocities caused by external contact torques are constrained in the null space of the other two task x_1 and x_2 with higher priorities. Regardless of the calculation error of null space projection matrices (J_1^\dagger , \bar{J}_2^\dagger and \bar{J}_3^\dagger), tasks with higher priorities are not disturbed by this compliance control scheme.

$$\dot{q}_c = J_1^\dagger \dot{x}_1 + \bar{J}_2^\dagger (\dot{x}_2 - J_2 J_1^\dagger \dot{x}_1) + \bar{J}_3^\dagger A'^{-1} (\tau_{ext} + K_d C_d^{-1} \int \tau_{ext} dt) \quad (26)$$

$$\text{where } \bar{J}_3^\dagger = (I - J_1^\dagger J_1)(I - \bar{J}_2^\dagger \bar{J}_2).$$

V. SINGULARITY AND JOINT LIMITS AVOIDANCE

Non-singularity and no joint limits (positions, velocities etc.) violations are assumed in the above sections. The problems of joint limits and singularity avoidance are often encountered in computer graphics and robotic applications, such as humanoid robots, exoskeleton, etc. Plenty of literature works have been reported to deal with these problems. Here, we have evaluated some of these methods and recommend several simple but effective solutions to fix this problem in the scenarios similar with ours in this paper.

A common used singularity robust algorithm is the Damped Least-Squares (DLS) technique [38], which is to solve the optimization problem of $\min_{\dot{q}} (\|\dot{x} - J\dot{q}\|^2 + \lambda^2 \|\dot{q}\|^2)$. $\lambda \in R$ is called the damping factor that means a trade-off between the least squares $\|\dot{x} - J\dot{q}\|^2$ and the minimum norm $\|\dot{q}\|^2$. The solution can be written as follows,

$$\dot{q} = J^T (JJ^T + \lambda^2 I)^{-1} \dot{x} \quad (27)$$

where $J^* = J^T (JJ^T + \lambda^2 I)^{-1}$ is damped pseudo-inverse, which can replace the general pseudo-inverse J^\dagger in recursive redundancy solution (11) and two viscoelastic models based compliance control expressions (18) and (24).

Another way to deal with singularity in this multi-priority framework is add a lower priority sub-task specialized to tackle this problem of kinematic and algorithmic singularities. Numerical studies on seven-degree-of-freedom redundant manipulator have been reported in [39], [40].

A simple and effective method to deal with the joint limits or constraints of joint range, velocity, acceleration and even joint torque is task scaling, which can reduce the speed and acceleration of a single or multiple task commands [41], [42]. A method named Saturation in the Null Space (SNS) is proposed to control the motion of redundant robots in a single task [43]. The authors also extend the SNS approach to multiple prioritized task cases [44]. In their work, the inequality constraints are emphasized and solved without violations, compared with other constrained optimization methods.

In our case, the DLS method expressed as (27) is adopted to prevent singularities. For joint limits avoidance, we propose a virtual spring approach to create a repelling torque τ_s to drive

TABLE 1. Joint limits of KUKA LBR iiwa 14 R820. [45].

	Range of motion	Maximum torque	Maximum velocity
J1	$\pm 170^\circ$	320Nm	$85^\circ/s$
J2	$\pm 120^\circ$	320Nm	$85^\circ/s$
J3	$\pm 170^\circ$	176Nm	$100^\circ/s$
J4	$\pm 120^\circ$	176Nm	$75^\circ/s$
J5	$\pm 170^\circ$	110Nm	$130^\circ/s$
J6	$\pm 120^\circ$	40Nm	$135^\circ/s$
J7	$\pm 175^\circ$	40Nm	$135^\circ/s$

away from joint limits, which is formulated as follows:

$$\tau_{s,i} = \begin{cases} \frac{\tau_{max,i}}{\sigma} (q_i - (q_{i,min} + \sigma)), & q_i < q_{i,min} + \sigma \\ 0, & q_{i,min} + \sigma \leq q_i \leq q_{i,max} - \sigma \\ \frac{\tau_{max,i}}{\sigma} (q_i - (q_{i,max} - \sigma)), & q_i > q_{i,max} - \sigma \end{cases} \quad (28)$$

where $\tau_{s,i}$ is to quantify repelling torques produced by virtual spring for each joint. $q_{i,max}$, $q_{i,min}$ denotes the i th maximum and minimum joint position limits, which depend on different robot manipulators and even vary from joints to joints of one robot. The neighborhood of each joint limits is quantified by a parameter σ , which measures the tolerance of distance to each joint limits. $\tau_{max,i}$ represent for the maximum joint actuation torques, which can be acquired from robot distributors and other artificial task constraints. From (28), we can infer that the repelling torque generated by virtual spring $\tau_{s,i}$ are zero when the joint configuration q_i are in the interval of $(q_{i,min} + \sigma \leq q_i \leq q_{i,max} - \sigma)$ and become larger and larger when approximating the joint torque limits $\tau_{max,i}$. Add the repelling torque of virtual spring to the proposed null space control law (19) and (30), the final expressions for two levels tasks are obtained as follows,

$$\dot{q}_c = J_1^\dagger \dot{x}_1 - (I - J_1^\dagger J_1) A^{-1} (\tau_{ext} + \tau_s) \quad (29)$$

$$\dot{q}_c = J_1^\dagger \dot{x}_1 - (I - J_1^\dagger J_1) A^{-1} (\tau_{ext} + K_d C_d^{-1} \int \tau_{ext} dt + \tau_s) \quad (30)$$

Similarly, the formulations for three levels prioritized tasks can be accordingly derived as (31) and (31).

$$\dot{q}_c = J_1^\dagger \dot{x}_1 + \bar{J}_2^\dagger (\dot{x}_2 - J_2 J_1^\dagger \dot{x}_1) + (I - J_1^\dagger J_1)(I - \bar{J}_2^\dagger \bar{J}_2) A^{-1} (\tau_{ext} + \tau_s) \quad (31)$$

$$\dot{q}_c = J_1^\dagger \dot{x}_1 + \bar{J}_2^\dagger (\dot{x}_2 - J_2 J_1^\dagger \dot{x}_1) + \bar{J}_3^\dagger A'^{-1} (\tau_{ext} + K_d C_d^{-1} \int \tau_{ext} dt + \tau_s) \quad (32)$$

$$\text{where } \bar{J}_3^\dagger = (I - J_1^\dagger J_1)(I - \bar{J}_2^\dagger \bar{J}_2).$$

VI. EXPERIMENT VERIFICATION AND DISCUSSION

A. EXPERIMENT SETUP AND PROCEDURES

The approaches we proposed have been implemented and practically evaluated on a KUKA[®] LBR iiwa 7 DOF redundant robot manipulator, which is shown in Fig. 3. The experiment setup is analogous to the concept of Fig. 1.

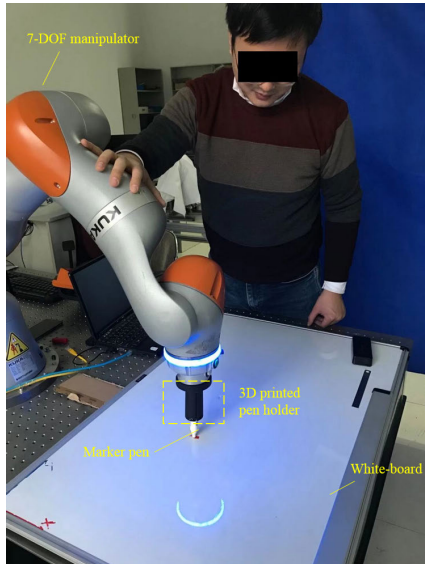


FIGURE 3. Experiment setup.

The communication between robot cabinet and our control PC is through the *Sunrise Connectivity* interface provided by the manufacturer KUKA GmbH. This interface allows users to directly servo control the robot manipulator and send position or velocity command streams up to $2 \sim 4$ ms. The joint limits of the KUKA iiwa 14 employed in our experiments are listed in Table 1 and used in (28) to calculate the torque of virtual spring $\tau_{s,i}, i = 1 \dots 7$. As emphasized in above sections, the methods proposed in this paper are general and manipulator independent, and not limited to the robot manipulator used in our experiments. Other robot manipulators are also applicable without any need of hardware changes.

As shown in Fig. 3, a flat office white board is fixed on the horizontal $X - Y$ plane relative to the robot base coordinates. In order to visualize the actual trajectory of end-effector, we use maker pens with different colors to draw the end-effector trajectories on the white board. Besides, in order to fasten these pens, we also made a fixture or holder, which is the black part attached to the robot flange in Fig. 3. The length of this holder is 80mm and cover the most part of the maker pens. A 3D-printed pen holder (in black) is designed and machined to attach the maker pen to the robot media *pneumatic-touch flange*.

The task assignments during our experiments are summarized in Table 2. In Case I, a desired circle tracking task of robot end-effector is carried out with no other extra tasks. Secondly, the same circle tracking task of end-effector is assigned as the 1st priority task while the 2nd priority task include several sub-cases. In Case II 1), the joint 1 (q_1) wagging task is chosen for better comparisons with following cases. Voigt and Maxwell model based null space compliance control methods (19) and (30) are assigned as 2nd prioritized task in Case II 2) and 3), respectively. Then, we increase the prioritized levels to three in case III. The desired circle tracking end-effector task is still chosen as the first level task

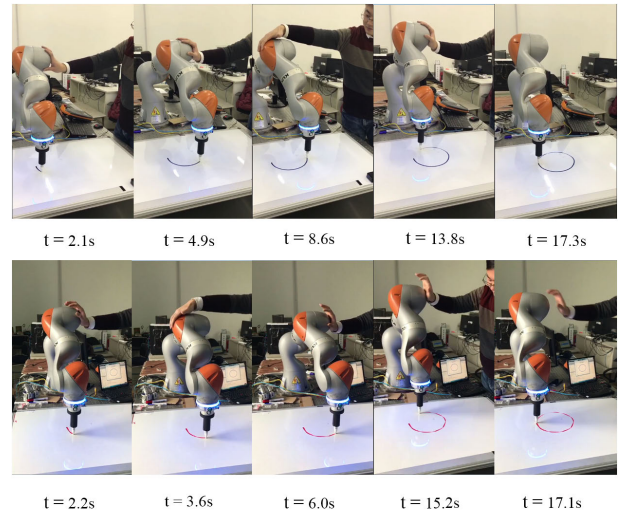


FIGURE 4. Snapshots of experiments: robot executing main task with human robot physical interaction.

and the joint 1 (q_1) wagging task is set as the second priority task, while the Voigt model and Maxwell model based null space compliance control (31) and (31) are assigned in the third priority level. For convenience, we denote these sub-cases as Roman numerals(I, II, III and etc.), each of which has been repeated ten times in our experiments. Some snapshots of experiment execution in one complete cycle are shown in Fig. 4. Experimental results and least square errors of the circle tracking (drawing) are analyzed, followed by a few comparisons and discussions. A supplementary video is attached for demonstration of our work and better understanding of readers. It is noteworthy that the drawing experiments are not industrial class (office white board, wear of pen and etc.), just for demo and visualization.

B. CASE I: ONLY CIRCLE TRACKING TASK

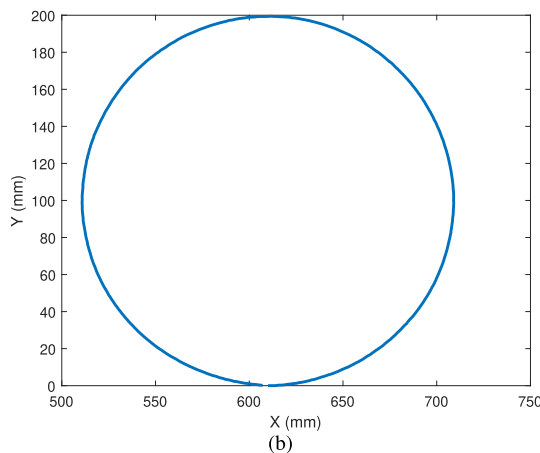
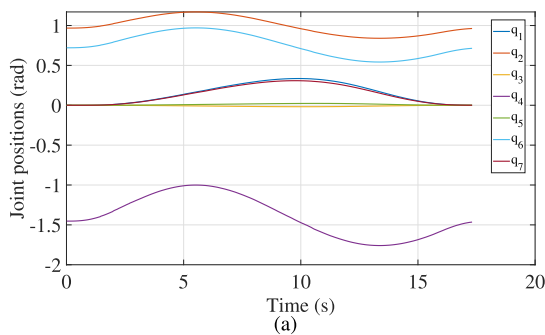
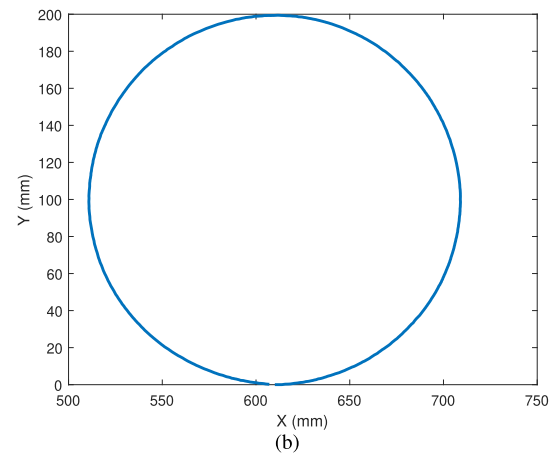
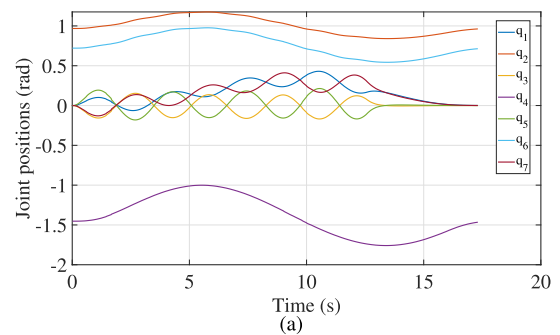
For better comparison, desired circle tracking tasks of robot end-effector have been carried out firstly. The radius of desired circle is 100mm in the $X - Y$ plane with a left direction($X+$) starting from the current Cartesian position of the pen-tool, which is $(610, 0, 8)\text{mm}$ in our experiments. The time history of joint positions is shown in Fig. 5(a), from which we can see that the actual joint positions move in a complete sinusoidal way. The resultant end-effector position in Cartesian space are shown in Fig. 5(b). In order to quantify the tracking errors during the experiments, we use the Least Squares errors between the desired circle and actually joint measurements. Same experiments have been repeated in ten times for each case, including the following subsections. The calculated errors are summarized and shown in Fig. 12 in subsection 6.5, which is an error-bar like figure.

C. CASE II: TWO LEVELS PRIORITIZED TASKS

In this subsection, two task levels are prioritized: the same circle tracking task is also set as the main task while

TABLE 2. Summary of task assignments in our experiments.

		1st level task	2nd level task	3rd level task	Denotations
Case I: one task	Only circle tracking	Circle tracking	None	None	I
Case II: two levels prioritized tasks	1) Joint 1 wagging	Circle tracking	Joint 1 wagging	None	II
	2) Voigt model based null space compliance	Circle tracking	Voigt model based null space compliance control	None	III
	3) Maxwell model based null space compliance	Circle tracking	Maxwell model based null space compliance control	None	IV
Case III: Three levels prioritized tasks	1) Voigt model based null space compliance	Circle tracking	Joint 1 wagging	Voigt model based null space compliance control	V
	2) Maxwell model based null space compliance	Circle tracking	Joint 1 wagging	Maxwell model based null space compliance control	VI

**FIGURE 5.** Case I: circle tracking task of end-effector only. (a) time history of joint positions during drawing the desired circle. (b) end-effector position in Cartesian space.**FIGURE 6.** Case II (1): joint 1 wagging task as second priority task. (a) time history of joint positions during drawing the desired circle. (b) end-effector position in Cartesian space.

three different null space tasks are chosen as the secondary priority task. We start from a desired sinusoidal joint 1 wagging task in the null space of the main circle task. Then, the typical Voigt model based null space compliance control is investigated for comparison with the Maxwell model based compliance control method we proposed. The desired viscoelastic coefficients in (19) and (30) are $M_d = \text{diag}[2, 2, 2]Ns^2/m$, $C_d = \text{diag}[60, 60, 60]Ns/m$, $K_d = \text{diag}[100, 100, 100]N/m$. Detailed experiments results are given as follows. Same as the above subsection, the tracking errors during experiments are summarized together in subsection 6.5.

1) JOINT 1 WAGGING

In this sub-case, the same circle tracking is assigned as robot main task while the desired sinusoidal trajectory of joint 1 is $q_{1d} = \frac{\pi}{3} \sin(2t)$. Generally, this joint wagging task is present here for two main purposes: one is for testing the accuracy of the numerical calculation of null space projection matrices ($I - J_1^\dagger J_1$, $I - \bar{J}_2^\dagger \bar{J}_2$ and etc.). Theoretically, robot main task will not be interfered by the null space projections. However, numerical calculation errors always exist in practical implementations. In our experiments, joint wagging task is added to evaluate whether the desired robot main task is affected or not. The other purpose is to compare with Case III

presented in the following subsection, in which the same joint 1 wagging task is chosen as the secondary level task.

The time history (lasted 17.3s) of joint positions and actual end-effector positions in $X - Y$ plane are shown in Fig. 6. From Fig. 6 (a), we can see that the joints $q_1 \cdots q_7$ move in a sinusoidal mode to make sure the end-effector follow the desired circle. The corresponding end-effector positions in $X - Y$ plane is given in Fig. 6 (b), which illustrates a circle with a radius of 100mm. Compared with Fig. 5 (b), these two circles are so similar that they are not distinguishable to the human naked eye. Comparisons of tracking error during the execution of different cases and discussions are given in following subsections.

2) VOIGT MODEL BASED NULL SPACE COMPLIANCE CONTROL

In Case II (2), the typical Voigt model based null space compliance control (19) is chosen as 2nd priority tasks. During the execution of robot tasks, human hands make contact on robot manipulator body randomly in a human robot physical interaction scenario, as illustrated in Fig. 1. As shown in Fig. 7, human makes six contacts on robot body, at 2.18s, 3.68s, 8.16s, 10.5s, 13.29s and 14.7s. The average duration of those six contacts are 0.48s. The amplitude of each estimated external torques caused by those human contacts vary from $-32.17Nm$ to $34.83Nm$. As shown in Fig. 7 (b), the resultant joint positions changes happen almost synchronous, at 2.24s, 3.69s, 8.2s, 10.52s, 13.36s and 14.74s. It is noteworthy that the changing directions are opposite to the external torque directions. For example, the joint 1 torque τ_1 caused by human contact happens at time 10.52s is nearly $25Nm$, and the corresponding position change of joint 1 q_1 goes downwards, similar in joints $q_1 \cdots q_7$. Human hands feel repulsive return forces simultaneously. In other words, the joint positions changes always against the direction of external torques, which verify the existence of repulsive forces always generated by Voigt model based compliance control methods. The experimental results are consistent with the theoretical analysis of the Voigt model in our former published works and Elastoplastic theories mentioned in *introduction* section.

3) MAXWELL MODEL BASED NULL SPACE COMPLIANCE CONTROL

In Case II (3), the first prioritized task is also the circle tracking task of end-effector, and the Maxwell model based null space compliance control law (30) as the second priority task. Similarly, human contact with robot body randomly. As shown in Fig. 8(a), human contact on robot body six times, at 2.01s, 4.18s, 6.38s, 9.79s, 12.9s and 15.08s. The average contact duration is 0.41s. The amplitude of each estimated external torques caused by those human contacts vary from $-45.37Nm$ to $41.62Nm$. The resultant joints positions are given in Fig. 8(b). The joint positions changes accordingly and happen at 2.07s, 4.21s, 6.51s, 9.86s, 12.98s and 15.12s. It is noteworthy that the changing directions of joint positions

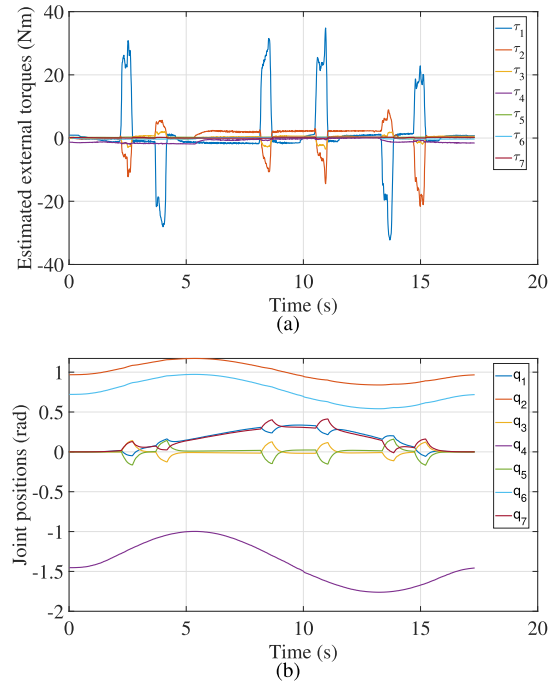


FIGURE 7. Case II (2): typical Voigt model based null space compliance control as second priority task. (a) estimated external torques. (b) time history of joint positions during task execution.

are coincide with the external torque directions. For example, the average of joint 1 torque happens at time 9.79s is nearly $23Nm$, and the corresponding position displacements of joint 1 at that time goes the same way. The magnitude of joint position displacements depend on the magnitude of external torques τ_{ext} plus their integral term $\int \tau_{ext} dt$. The annoying elastic return forces in Voigt model Case II (2) are removed, due to the characteristics of Maxwell model. Therefore, human feel more comfortable than the Voigt model base. In other words, the whole body compliance changes from elastic to plastic while the robot main task remains undisturbed by using the Maxwell model based approaches.

D. CASE III: THREE LEVELS PRIORITIZED TASKS

In this subsection, a third level prioritized task are added to make robot tasks more versatile. In Case III, the desired circle tracking task is still set as the first level and main task, the joint 1 wagging task in previous subsection is chosen as the second prioritized task, and the two viscoelastic models based null space compliance control methods (31) and (31) are assigned as the third priority task, respectively. The desired viscoelastic coefficients M_d , C_d and K_d are same as Case II. Similarly, each sub-cases have been carried out for ten times.

1) VOIGT MODEL BASED NULL SPACE COMPLIANCE CONTROL

As shown in Fig. 9 (a), a human made five contacts on robot body during the main drawing task execution, at 2.29s, 5.31s,

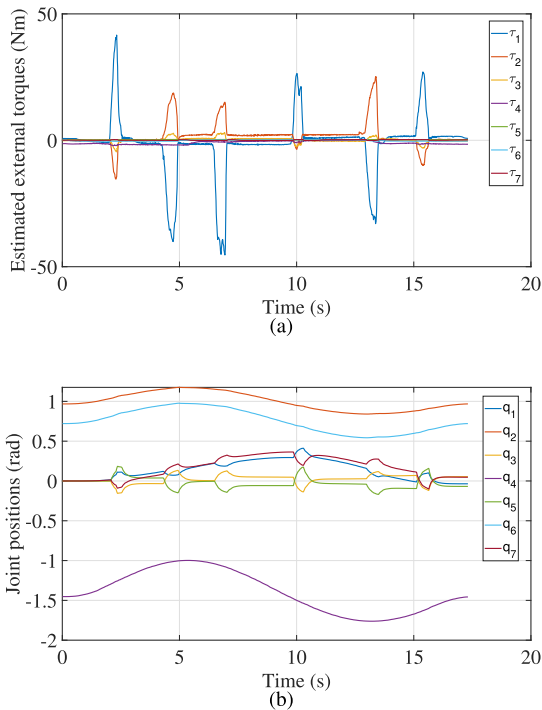


FIGURE 8. Case II (3): Maxwell model based null space compliance control as second priority task. (a) estimated external torques. (b) time history of joint positions during task execution.

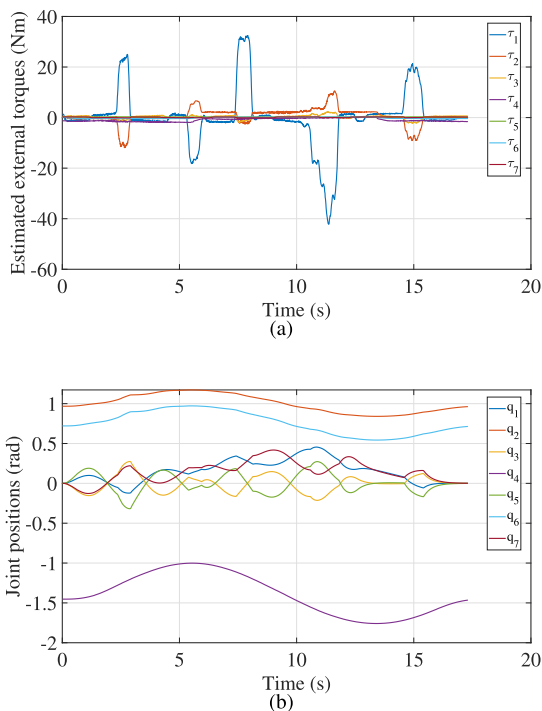


FIGURE 9. Case III (1): typical Voigt model based null space compliance control as third priority task. (a) estimated external torques. (b) time history of joint positions during task execution.

7.33s, 10.18s and 14.51s. The amplitude of each estimated external torques caused by those human contacts vary from

–41.88Nm to 32.3Nm. The resultant joints positions are given in Fig. 9 (b). The joint positions changes accordingly and happen afterwards at 2.37s, 5.39s, 7.42s, 10.57s and 14.6s. It should be emphasized that the changing directions are opposite to the external torque directions. Compared with two levels tasks in Case II, the repulsive return forces are also generated while the robot main task remains unaffected so much. However, the wagging movement of joint 1 increase the task levels and complexity of robot tasks.

2) MAXWELL MODEL BASED NULL SPACE COMPLIANCE CONTROL

In Case III 2), human contacts happen at 2.72s, 5.68s, 9.36s, 11.95s and 15.35s in Fig. 10 (a). The time durations of those contacts are averaged as 0.41s. The amplitude of each estimated external torques caused by those human contacts vary from –30.95Nm to 28.89Nm. The resultant joints position displacements are given in Fig. 8(b). The resultant joint positions changes at 2.84s, 5.8s, 9.85s, 12.03s and 15.45s. It is noteworthy that the changing directions are coincide with the external torque directions. The magnitude of joint positions changes depend on the magnitude of external torques τ_{ext} plus their integral term $\int \tau_{ext} dt$. Compared with two levels prioritized tasks in Case II 3), more task levels are added to demonstrate the effectiveness of the proposed methods. Also the whole body compliance changes to plastic not elastic in Case II 3) and human comfortableness get improved, compared with typical Voigt model based null space compliance in previous sections.

E. EXPERIMENT RESULTS AND COMPARISON

In order to visualize the circle tracking task of robot end-effector, we are inspired to attach a marker pen to the *Media touch and pneumatic flange* and then draw those circles on a office white board. Some snapshots of the marker pen drawing experiment results are shown in Fig. 11. For each case, we use a different colorful marker pens: black for case I, blue and red for case II and III, respectively. The error-bar like figure to quantify the drawing errors is given in Fig. 12. The x – $axis$ compose of six sub-cases, which are denoted as Roman numerals(i.e. I, II, III, IV, V, VI). The specific correspondence can be found in Table 2, the last column which is *Denotations*. The y – $axis$ indicates the statistical errors of the six cases repeated in ten times each. For example, in case III, the mean value of least square tracking errors in ten repetitive experiments is $2.81 \times 10^{-5}m$ whereas the maximum is $2.93 \times 10^{-5}m$ and the minimum is $2.734 \times 10^{-5}m$. In case V, the mean value of ten times tracking experiments is $4.61 \times 10^{-5}m$ whereas the maximum is $4.673 \times 10^{-5}m$ and the minimum is $4.484 \times 10^{-5}m$. Comparisons of the six cases indicate that the tracking errors of robot main task grow larger as the task prioritized levels increasing (from one level to three levels), because the numerical calculations burdens of different cases grow with the prioritized task levels. In general, tracking errors of the robot main task are acceptable (the magnitude position tracking accuracy of our collaborative robot usually

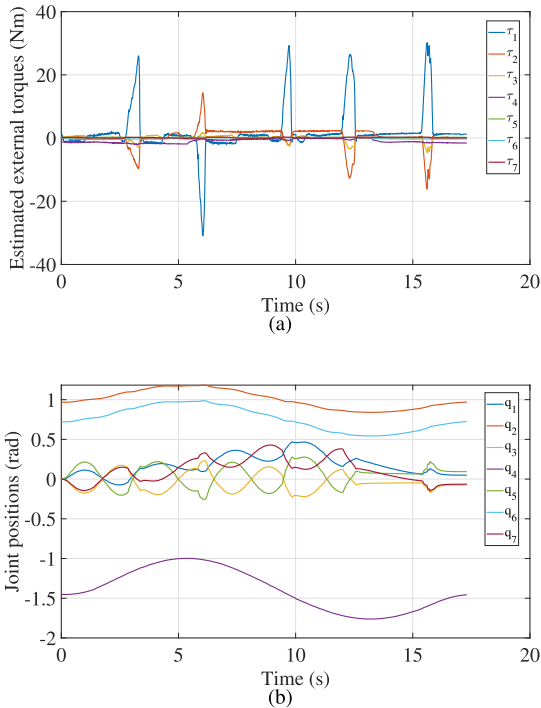


FIGURE 10. case III (2): Maxwell model based null space compliance control as third priority task. (a) estimated external torques. (b) time history of joint positions during task execution.

$\approx \pm 0.5mm$ by our Leica[®] laser tracker system), so the continuity and quality of the robot’s task can be maintained. It is noteworthy that the practical tracking error of robot main task may depend on the mechanical wear of robot, the calculating ability of control PC and etc.

The differences between Voigt and Maxwell model based null space compliance methods are verified by experiment results. As concluded in previous subsections, repelling forces are always generated in the opposite direction of human contact forces, due to the spring dominant interconnections of Voigt model. Therefore, human feels these return forces every time human contact on robot body. Human safety and comfortableness may be harmed due to these inevitable elastic return forces. On the contrary, the annoying and harmful return forces are removed by the Maxwell model based null space compliance control approach proposed in this paper. As a result, human feels no antagonistic return forces when human contact forces apply on the whole body of robot, thanks to the exploited advantages of Maxwell model on contact reducing and impact absorption. Last but not least, the resultant joint displacements in null space of robot main task depend on the history of external torques, due to the integral term $\int \tau_{ext} dt$. In other words, the resultant null space joint positions vary with different experiment attempts. However, these null space displacements do not interfere the execution of robot main task. In summary, compared with typical Voigt model based compliance control, the Maxwell model based methods we proposed ensue the robot manipulators a

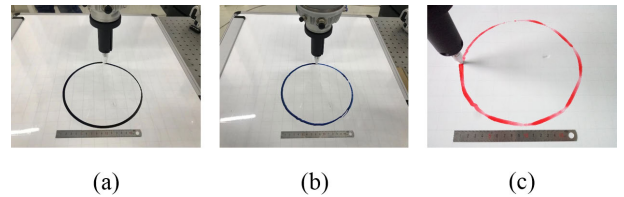


FIGURE 11. Snapshots of marker pen drawing experiment results. (a) Case I: drawing task only. (b) Case II: two prioritized tasks. (c) Case III: three prioritized tasks.

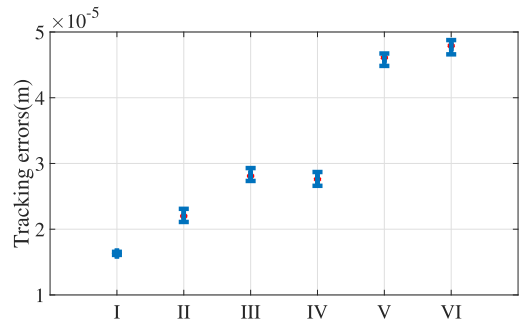


FIGURE 12. Least square errors of ten times experiments for each cases.

new type of, general and cushion-like whole body compliance, which makes robot more safe and human friendly.

F. DISCUSSION

As emphasized in previous section, Maxwell model based compliance control is a quite new topic. The methods we proposed exploit the advantages of Maxwell model and can be used in human robot physical interaction related research. Based on related literature review and our experimental experience, several discussions are given in this subsection to provide a potential help for follow up study.

1) The necessity and importance of external torque estimation can never be overemphasized. This relationship between the estimated torque and joint displacements is the desired compliance. The external torque estimation is a premise for the calculation of joint displacements, see (17) and (23). In other scenarios, the convergence rate and task error can be significantly reduced by using the external torque observer [46]. It is worthwhile to mention that the external torque estimation can be realized through other methods. A task error-based disturbance observer is adopted and compared with the common used momentum-based observer on task error reducing [36].

2) Form the results of experiments we experienced, tracking errors grow slightly with the task prioritized levels, due to frequent numerical calculation of genera inverse matrices J_i^\dagger and projection matrices P_i^A . As shown in Figure 12, the task least square errors of three levels prioritized tasks with an average of $4.7 \times 10^{-5}m$ are nearly two times bigger than two levels cases, because of the increasing numerical calculations. The closed-loop inverse kinematics (CLIK) algorithm can come to remedy the closed-loop main task accuracy [47].

3) The methods investigated in this paper are based on the first-order redundancy resolutions. Acceleration information and robot dynamics can also be exploited to realized more complex tasks [46], [48]. But there may add extra requirements on robot controllers, such as torque controllers. If so, they are not so general and manipulator independent as our methods.

VII. CONCLUSION AND FUTURE WORK

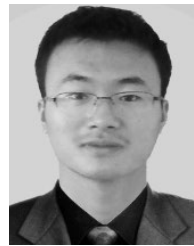
In order to propose a solution to the challenging problem of ensuring a whole body compliance behavior for the sake of human safety and meanwhile keeping the main task of end-effector undisturbed, a recursive first-order redundancy resolution is generalized. Moreover, for the purpose of exploiting the superior performance on contact reducing and impact absorption, a novel Maxwell model based null space compliance control scheme is proposed and practically realized in the multi-prioritized task framework. Compared with typical Voigt model based compliance control also in the multi-priority framework, the annoying and even harmful elastic return forces are removed and human comfortableness can be improved. To the best of the author's knowledge, this paper is the first one reported on this topic at present. Our work have a promising usage in human physical interaction scenarios and can possibly inspire other research on this topic.

Future works mainly includes: in order to deal with the complexity and uncertainty of human robot interaction, more theoretical research on adaptive or variable compliance control based on Maxwell model are needed and also considered as our ongoing work. Moreover, apart from the scenarios demonstrated in this paper, the practical application of Maxwell model based compliance control methods can be extended to other robotic research areas such as human robot co-assembling, robot surgery and etc.

REFERENCES

- [1] M. Peshkin and J. E. Colgate, "Cobots," *Ind. Robot.*, vol. 26, no. 5, pp. 335–341, 1999.
- [2] L. Huo and L. Baron, "The joint-limits and singularity avoidance in robotic welding," *Ind. Robot. Int. J.*, vol. 35, no. 5, pp. 456–464, Aug. 2008.
- [3] H. Su, C. Yang, G. Ferrigno, and E. De Momi, "Improved human-robot collaborative control of redundant robot for teleoperated minimally invasive surgery," *IEEE Robot. Autom. Lett.*, vol. 4, no. 2, pp. 1447–1453, Apr. 2019.
- [4] H. Su, J. Sandoval, M. Makhdoumi, G. Ferrigno, and E. De Momi, "Safety-enhanced human-robot interaction control of redundant robot for teleoperated minimally invasive surgery," in *Proc. IEEE Int. Conf. Robot. Autom. (ICRA)*, May 2018, pp. 6611–6616.
- [5] H. Su, W. Qi, C. Yang, A. Aliverti, G. Ferrigno, and E. De Momi, "Deep neural network approach in human-like redundancy optimization for anthropomorphic manipulators," *IEEE Access*, vol. 7, pp. 124207–124216, 2019.
- [6] S. Chiaverini, B. Siciliano, and O. Egeland, "Kinematic analysis and singularity avoidance for a seven-joint manipulator," in *Proc. Amer. Control Conf.*, May 1990, pp. 2300–2305.
- [7] A. De Luca, G. Oriolo, and P. R. Giordano, "Kinematic modeling and redundancy resolution for nonholonomic mobile manipulators," in *Proc. IEEE Int. Conf. Robot. Autom. (ICRA)*, May 2006, pp. 1867–1873.
- [8] J. Baillieul, "Kinematic programming alternatives for redundant manipulators," in *Proc. IEEE Int. Conf. Robot. Autom.*, vol. 2, Mar. 1985, pp. 722–728.
- [9] P. Chang, "A closed-form solution for inverse kinematics of robot manipulators with redundancy," *IEEE J. Robot. Autom.*, vol. JRA-3, no. 5, pp. 393–403, Oct. 1987.
- [10] J. Hollerbach and K. Suh, "Redundancy resolution of manipulators through torque optimization," *IEEE J. Robot. Autom.*, vol. 3, no. 4, pp. 308–316, Aug. 1987.
- [11] Y. Nakamura, H. Hanafusa, and T. Yoshikawa, "Task-priority based redundancy control of robot manipulators," *Int. J. Robot. Res.*, vol. 6, no. 2, pp. 3–15, Jun. 2016.
- [12] A. Albu-Schaffer, O. Eiberger, M. Grebenstein, S. Haddadin, C. Ott, T. Wimbock, S. Wolf, and G. Hirzinger, "Soft robotics," *IEEE Robot. Autom. Mag.*, vol. 15, no. 3, pp. 20–30, Sep. 2008.
- [13] S. Wolf and G. Hirzinger, "A new variable stiffness design: Matching requirements of the next robot generation," in *Proc. IEEE Int. Conf. Robot. Autom.*, May 2008, pp. 1741–1746.
- [14] A. Bicchi and G. Tonietti, "Fast and 'soft-arm' tactics [robot arm design]," *IEEE Robot. Autom. Mag.*, vol. 11, no. 2, pp. 22–33, Jun. 2004.
- [15] G. Grioli, S. Wolf, M. Garabini, M. Catalano, E. Burdet, D. Caldwell, R. Carloni, W. Friedl, M. Grebenstein, and M. Laffranchi, "Variable stiffness actuators: The user's point of view," *Int. J. Robot. Res.*, vol. 34, no. 6, pp. 727–743, 2015.
- [16] N. Hogan, "Impedance control: An approach to manipulation," in *Proc. Amer. Control Conf.*, Jul. 1984, pp. 304–313.
- [17] C. Ott, R. Mukherjee, and Y. Nakamura, "Unified impedance and admittance control," in *Proc. IEEE Int. Conf. Robot. Autom.*, May 2010, pp. 554–561.
- [18] F. J. Abu-Dakka, L. Rozo, and D. G. Caldwell, "Force-based variable impedance learning for robotic manipulation," *Robot. Auto. Syst.*, vol. 109, pp. 156–167, Nov. 2018.
- [19] Z. Li, J. Liu, Z. Huang, Y. Peng, H. Pu, and L. Ding, "Adaptive impedance control of human-robot cooperation using reinforcement learning," *IEEE Trans. Ind. Electron.*, vol. 64, no. 10, pp. 8013–8022, Oct. 2017.
- [20] G. Peng, C. Yang, W. He, and C. L. P. Chen, "Force sensorless admittance control with neural learning for robots with actuator saturation," *IEEE Trans. Ind. Electron.*, vol. 67, no. 4, pp. 3138–3148, Apr. 2020.
- [21] C. Yang, G. Peng, L. Cheng, J. Na, and Z. Li, "Force sensorless admittance control for teleoperation of uncertain robot manipulator using neural networks," *IEEE Trans. Syst., Man, Cybern., Syst.*, to be published.
- [22] A. D. Drozdov, *Mechanics of Viscoelastic Solids*. Hoboken, NJ, USA: Wiley, 1998.
- [23] D. Mewes and F. Mauser, "Safeguarding crushing points by limitation of forces," *Int. J. Occupational Saf. Ergonom.*, vol. 9, no. 2, pp. 177–191, Jan. 2015.
- [24] Y. Yamada, K. Saita, H. Ikeda, N. Sugimoto, H. Miura, and H. Nakamura, "Evaluation of pain tolerance based on a biomechanical method for human-robot Coexistence," *Trans. Jpn. Soc. Mech. Eng. C*, vol. 63, no. 612, pp. 2814–2819, 1997.
- [25] *Robots and Robotic Devices—Collaborative Robots*, International Standard ISO/TS 15066:2016, International Organization for Standardization, Feb. 2016.
- [26] W. Fliigg, *Viscoelasticity*. London, U.K.: Blaisdell, 1967, pp. 1069–1084.
- [27] J. Lubliner, *Plasticity Theory*. Chelmsford, MA, USA: Courier Corporation, 2008.
- [28] I. I. Argatov, "Mathematical modeling of linear viscoelastic impact: Application to drop impact testing of articular cartilage," *Tribol. Int.*, vol. 63, pp. 213–225, Jul. 2013.
- [29] T. Senoo, M. Koike, K. Murakami, and M. Ishikawa, "Visual shock absorber based on Maxwell model for anti-rebound control," in *Proc. IEEE/RSJ Int. Conf. Intell. Robots Syst. (IROS)*, Sep. 2015, pp. 1640–1645.
- [30] L. Fu, R. Wu, and J. Zhao, "On the stability of maxwell model based impedance control and Cartesian admittance control implementation," in *Proc. IEEE 4th Int. Conf. Adv. Robot. Mechatronics (ICARM)*, Jul. 2019, pp. 793–798.
- [31] J. W. Jeong and P. H. Chang, "A task-priority based framework for multiple tasks in highly redundant robots," in *Proc. IEEE/RSJ Int. Conf. Intell. Robots Syst.*, Oct. 2009, pp. 5886–5891.
- [32] A. Wahrburg, J. Bos, K. D. Listmann, F. Dai, B. Matthias, and H. Ding, "Motor-Current-Based estimation of Cartesian contact forces and torques for robotic manipulators and its application to force control," *IEEE Trans. Autom. Sci. Eng.*, vol. 15, no. 2, pp. 879–886, Apr. 2018.
- [33] J. Jung, J. Lee, and K. Huh, "Robust contact force estimation for robot manipulators in three-dimensional space," *Proc. Inst. Mech. Eng., C, J. Mech. Eng. Sci.*, vol. 220, no. 9, pp. 1317–1327, Aug. 2016.

- [34] H. Cho, M. Kim, H. Lim, and D. Kim, "Cartesian sensor-less force control for industrial robots," in *Proc. IEEE/RSJ Int. Conf. Intell. Robots Syst.*, Sep. 2014, pp. 4497–4502.
- [35] A. De Luca and R. Mattone, "Actuator failure detection and isolation using generalized momenta," in *Proc. IEEE Int. Conf. Robot. Autom.*, vol. 1, Sep. 2003, pp. 634–639.
- [36] H. Sadeghian, L. Villani, M. Keshmiri, and B. Siciliano, "Task-space control of robot manipulators with null-space compliance," *IEEE Trans. Robot.*, vol. 30, no. 2, pp. 493–506, Apr. 2014.
- [37] C. Ott, *Cartesian Impedance Control of Redundant and Flexible-Joint Robots*. Berlin, Germany: Springer-Verlag, 2008.
- [38] Y. Nakamura and H. Hanafusa, "Inverse kinematic solutions with singularity robustness for robot manipulator control," *J. Dyn. Syst., Meas., Control*, vol. 108, no. 3, pp. 163–171, Sep. 1986.
- [39] S. Chiaverini, "Singularity-robust task-priority redundancy resolution for real-time kinematic control of robot manipulators," *IEEE Trans. Robot. Autom.*, vol. 13, no. 3, pp. 398–410, Jun. 1997.
- [40] S. B. Slotine, "A general framework for managing multiple tasks in highly redundant robotic systems," in *Proc. 5th Int. Conf. Adv. Robot.*, vol. 2, 1991, pp. 1211–1216.
- [41] P. Chiacchio and S. Chiaverini, "Coping with joint velocity limits in first-order inverse kinematics algorithms: Analysis and real-time implementation," *Robotica*, vol. 13, no. 5, pp. 515–519, Mar. 2009.
- [42] G. Antonelli, S. Chiaverini, and G. Fusco, "A new on-line algorithm for inverse kinematics of robot manipulators ensuring path tracking capability under joint limits," *IEEE Trans. Robot. Autom.*, vol. 19, no. 1, pp. 162–167, Feb. 2003.
- [43] F. Flacco, A. De Luca, and O. Khatib, "Motion control of redundant robots under joint constraints: Saturation in the null space," in *Proc. IEEE Int. Conf. Robot. Autom.*, May 2012, pp. 285–292.
- [44] F. Flacco, A. De Luca, and O. Khatib, "Prioritized multi-task motion control of redundant robots under hard joint constraints," in *Proc. IEEE/RSJ Int. Conf. Intell. Robots Syst.*, Oct. 2012, pp. 3970–3977.
- [45] KUKA Robotics GmbH, *KUKA LBR iiwa Brochure (EN)*. [Online]. Available: <http://www.kuka.com>
- [46] A. Karami, H. Sadeghian, M. Keshmiri, and G. Oriolo, "Force, orientation and position control in redundant manipulators in prioritized scheme with null space compliance," *Control Eng. Pract.*, vol. 85, pp. 23–33, Apr. 2019.
- [47] P. Chiacchio, S. Chiaverini, L. Sciacivco, and B. Siciliano, "Closed-loop inverse kinematics schemes for constrained redundant manipulators with task space augmentation and task priority strategy," *Int. J. Robot. Res.*, vol. 10, no. 4, pp. 410–425, Jul. 2016.
- [48] C. Ott, A. Dietrich, and A. Albu-Schäffer, "Prioritized multi-task compliance control of redundant manipulators," *Automatica*, vol. 53, pp. 416–423, Mar. 2015.



LE FU received the B.S. degree from the Henan University of Science and Technology, Luoyang, China, and the M.S. degree in mechanical engineering from the Harbin Institute of Technology, Harbin, China, where he is currently pursuing the Ph.D. degree with the State Key Laboratory of Robotics and System. His research interests include human–robot interaction and collaboration, robotic learning, and cooperative manipulation.



JIE ZHAO received the B.S., M.S., and Ph.D. degrees in mechatronics engineering from the Harbin Institute of Technology, Harbin, China, in 1990, 1993, and 1996, respectively. He is currently a Full Professor with the School of Mechatronics Engineering and the Director of the State Key Laboratory of Robotics and System, Harbin Institute of Technology. He has been honored as the Changjiang Scholars Distinguished Professor. He also serves as the Director of the Institute of Robotics, Harbin Institute of Technology, and the Leader of the National Expert Group on Intelligent Robots, National Natural Science Foundation of China. He has published one book and more than 280 articles in major international journals and conferences, which cited more than 780 times. His research interests include teleoperation robotic systems, robots serve in extreme environments, industrial robots and control, human–robot collaboration, and bionic robots.

• • •